
Coupled Physics-Based and Machine Learning Streamflow Modeling with High-Resolution Flood Inundation and Impact Assessment for Hurricane Florence (2018): A Case Study of the Neuse River at Goldsboro, North Carolina

H M Ashaduzzaman[1]

[1]Independent Researcher

ORCID iD: https://orcid.org/0000-0003-0292-404X

Corresponding author email: hmasad09@gmail.com

Code and data-processing scripts: https://github.com/asadpstu/hurricane-florence

---

Coupled Physics-Based and Machine Learning Streamflow Modeling with High-Resolution Flood Inundation and Impact Assessment for Hurricane Florence (2018): A Case Study of the Neuse River at Goldsboro, North Carolina

H M Ashaduzzaman*[1]

[1]Independent Researcher

Abstract

Hurricane Florence made landfall in North Carolina in September 2018 and produced record or near-record river stages across the Neuse River basin, including at United States Geological Survey (USGS) gauge 02089000 near Goldsboro. This study presents an end-to-end hydrological and flood-mapping workflow that couples a semi-distributed, physics-based rainfall-runoff model (Physics V3.5) and a gradient-boosted machine learning model (ML V4, based on Extreme Gradient Boosting) to predict discharge at the Goldsboro gauge, converts predicted and observed discharge to stage through an event-effective, hysteresis-aware stage-discharge (H-Q) surrogate, and produces spatially explicit flood-extent and flood-depth maps using a 1 m light detection and ranging (lidar) digital elevation model (DEM). The upstream contributing watershed ($\approx$6,232 km^2) was delineated using the USGS Network-Linked Data Index and the National Hydrography Dataset Plus High Resolution and discretized into 37 routed subcatchments. Physics V3.5 was developed using five historical calibration events (2015–2016) and three temporal-check events (2017), with Hurricane Florence withheld from parameter optimization; ML V4 was trained on 2015–2016 data and validated on the same 2017 events using only exogenous rainfall and routing features, with no observed-discharge lag or recursive predicted-discharge inputs. The stage-discharge surrogate uses isotonic (monotonic) regression fitted independently to each limb after robust aggregation of repeated stage values, and ML V4 draws on 40 engineered, purely exogenous rainfall-routing features selected from a ten-candidate hyperparameter grid using a composite skill score. Over the 14–23 September 2018 evaluation window, Physics V3.5 achieved a lower mean absolute error than ML V4 for both daily discharge (82.3 vs. 103.6 m^3 s^{-1}) and daily stage (1.03 vs. 2.01 ft), and both models reproduced the timing of the observed discharge peak on 18 September 2018; the retained Physics V3.5 artifact additionally reports an approximate whole-event Nash–Sutcliffe efficiency of 0.887 and Kling–Gupta efficiency of 0.831, although – as the artifact's own provenance record makes explicit – Florence's observed discharge contributed to that model's parameter selection, so this figure is not an independent validation statistic in the way the ML V4 result is. The validated discharge series were converted to a spatial water-surface elevation profile along the Neuse River mainstem using a robust, iteratively re-weighted longitudinal regression, compared against the lidar DEM under a morphological hydraulic-connectivity constraint, and combined with WorldPop, National Land Cover Database, and OpenStreetMap layers – overlaid as fractional, sub-pixel coverage rather than a binary mask – to estimate population, land-cover, road, and facility exposure in the Goldsboro area of interest. The results illustrate both the value and the limitations of combining conceptual hydrology with data-driven discharge prediction for extreme, data-scarce flood events, and the importance of transparent gap-handling, extrapolation, and validation-independence rules in operational flood-mapping workflows.

*Corresponding author. Email: hmasad09@gmail.com. ORCID: https://orcid.org/0000-0003-0292-404X.
Code and data-processing scripts: https://github.com/asadpstu/hurricane-florence

Keywords: Hurricane Florence; Neuse River; flood inundation mapping; stage-discharge relationship; semi-distributed hydrological model; XGBoost; digital elevation model; flood exposure assessment

Table 1: Nomenclature and abbreviations.

Term	Meaning	Term	Meaning
AOI	Area of interest	NAVD88	North American Vertical Datum of 1988
DEM	Digital elevation model	NLCD	National Land Cover Database
ET_0	Reference evapotranspiration	NLDI	Network-Linked Data Index
FAO-56	FAO reference ET_0 method	NSE	Nash–Sutcliffe efficiency
FIM	Flood inundation mapping	NWIS	National Water Information System
H	Gauge stage (height)	OSM	OpenStreetMap
HAND	Height above nearest drainage	PBIAS	Percent bias
H-Q	Stage-discharge relationship	Q	Discharge
KGE	Kling–Gupta efficiency	QPE	Quantitative precipitation estimate
MAE	Mean absolute error	RMSE	Root-mean-square error
MAD	Median absolute deviation	USGS	United States Geological Survey
MRMS	Multi-Radar Multi-Sensor	UTC	Coordinated Universal Time
NHDPlus HR	National Hydrography Dataset Plus High Resolution	WSE	Water-surface elevation
		XGBoost	Extreme Gradient Boosting

1. Introduction

Hurricane Florence made landfall near Wrightsville Beach, North Carolina, on 14 September 2018 and stalled over the state for several days, producing some of the highest storm-total rainfall accumulations recorded in the eastern United States. The resulting runoff caused prolonged and, in many reaches, record river flooding across the Coastal Plain of North Carolina, including along the Neuse River at Goldsboro, Wayne County. Predicting and mapping such extreme, slow-evolving flood events requires (i) a reliable estimate of river discharge during and immediately after the storm, (ii) a robust and physically consistent method for converting discharge to a spatially varying water-surface elevation, and (iii) an assessment of the population, infrastructure, and land cover exposed to the resulting inundation.

Two broad families of methods are commonly used to predict river discharge during extreme events: conceptual or physically based rainfall-runoff models, which represent watershed storage, runoff generation, and channel routing explicitly, and data-driven or machine learning models, which learn a statistical mapping between forcing variables and observed discharge. Each approach carries distinct advantages and risks when applied to an extreme, largely out-of-sample event such as Hurricane Florence: physically based models can extrapolate more gracefully beyond the calibration range but depend on the fidelity of their parameterizations, while machine learning models can capture complex nonlinear relationships but are more prone to degraded performance when asked to extrapolate to conditions not well represented in their training data.

This paper documents a combined workflow, developed for the Neuse River at USGS gauge 02089000

(Goldsboro, NC), that (1) builds an event-effective stage-discharge (H-Q) surrogate directly from observed Hurricane Florence hydrometric data, explicitly separating the rising and falling limbs of the flood hydrograph; (2) develops and compares two independent discharge-prediction models – a semi-distributed physically based model ("Physics V3.5") and a gradient-boosted regression model ("ML V4") – under a strict temporal calibration/validation design that withholds Hurricane Florence from both models' parameter selection processes; (3) converts the resulting discharge time series into a spatially distributed flood-depth and flood-extent product using a 1 m lidar DEM and a hydraulic-connectivity rule; and (4) quantifies the population, land-cover, and infrastructure exposure associated with the mapped flood extent. The specific objectives of the study are to (a) present a reproducible, well-documented data and modeling pipeline for extreme-event flood mapping in a data-scarce, single-gauge setting, (b) compare the performance of the physically based and machine learning discharge models against observed Hurricane Florence hydrometric data, and (c) discuss the practical and scientific limitations of the workflow, including gaps in the forcing data record, the absence of an authoritative historical rating curve for the event, and the use of contemporaneous but not necessarily event-synchronous exposure datasets.

2. Study Area and Data

2.1 Study area

The study focuses on the Neuse River watershed upstream of USGS streamgage 02089000 (Neuse River near Goldsboro, North Carolina; approximate coordinates 35.3375°N, 77.9975°W). The USGS-published drainage area at this gauge is 2,399 mi^2, corresponding to an independently delineated contributing area of approximately 6,232 km^2 in this study. The gauge reference elevation used to convert stage to a geodetic water-surface elevation is 41.926 ft in the North American Vertical Datum of 1988 (NAVD88), taken from National Oceanic and Atmospheric Administration/National Weather Service (NOAA/NWS) flood inundation mapping metadata for the site. Flood mapping and impact assessment were performed within a smaller, locally defined area of interest (AOI) surrounding Goldsboro, which is distinct from – and always kept separate from – the much larger upstream hydrologic contributing area (Figure 1). Daily flood products were generated for the ten-day window of 14–23 September 2018, spanning the rise, peak, and recession of the Hurricane Florence flood wave at the gauge.

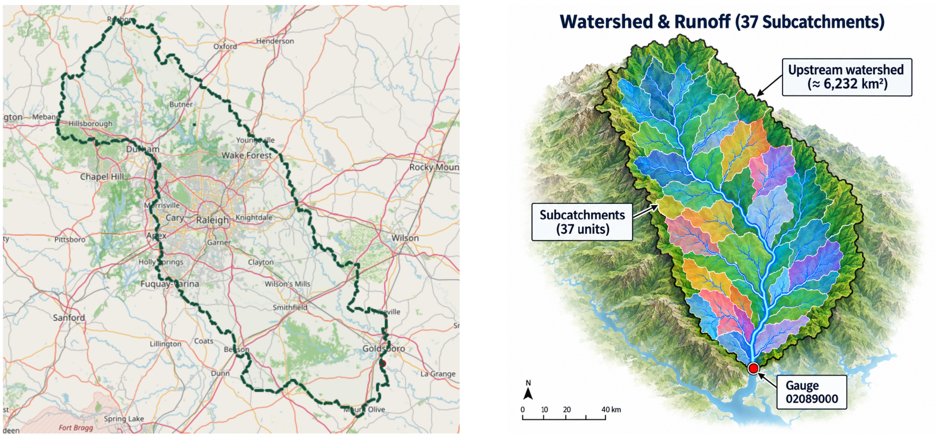

Figure 1: Left: upstream watershed contributing to USGS gauge 02089000, delineated using the USGS Network-Linked Data Index. Right: conceptual representation of the upstream watershed (≈6,232 km^2) discretized into 37 connected routing subcatchments draining to the Goldsboro gauge.

2.2 Data sources and temporal coverage

Table 2 summarizes the primary datasets used in the study, their role in the workflow, and the date ranges or epochs over which each was acquired. Each dataset was assigned a single, clearly defined role, and observation, precipitation, terrain, and exposure sources were kept in separate processing streams throughout the workflow.

Table 2: Primary data sources, their role in the workflow, and the date ranges or epochs used.

Source / dataset	Role	Date range / epoch
USGS National Water Information System (NWIS)	Florence discharge/stage, rating information, and field measurements at gauge 02089000	Event: 10–25 Sep 2018; forcing: 1–26 Sep 2018
USGS Network-Linked Data Index (NLDI)	Upstream watershed geometry, accepted only after gauge-location and drainage-area quality control	Current basin delineation service
USGS NHDPlus High Resolution (HU4 0302)	Flowlines, raw catchments, and downstream routing used to build 37 modelling subcatchments	No event time window required
NOAA/NCEP Multi-Radar Multi-Sensor (MRMS) system	Hourly quantitative precipitation estimates for Florence and a 2015–2017 model-development archive	Florence: 1–27 Sep 2018; historical: 10 May 2015–1 Jan 2018; warm-up: 1 Jun–27 Sep 2018
ERA5-Land (Copernicus Climate Data Store)	Antecedent soil/deep wetness and meteorology for Physics V3.5 state and reference evapotranspiration	Development: 1 Jan 2015–1 Jan 2018 (45-day antecedent windows); Florence state: 1 Jun–26 Sep 2018
2014 lidar DEM	1 m NAVD88 terrain used by the production flood mapper	2014 terrain product
Named Neuse River mainstem	Hydrographic reference for the longitudinal water-surface-elevation profile through the Goldsboro reach	–
NOAA FIM / Advanced Hydrologic Prediction Service (AHPS)	Small-domain reference flood-inundation layer, used only for qualitative comparison, not for production mapping	–
Copernicus Emergency Management Service (EMSR311)	Used only to recover the published Goldsboro analysis AOI boundary	–
WorldPop (2018), National Land Cover Database (NLCD, 2016), OpenStreetMap (OSM)	Population, land cover/imperviousness, buildings, roads, and facilities for impact assessment	WorldPop 2018; NLCD 2016; OSM current at acquisition time

2.3 Data-gap handling

Historical MRMS precipitation records were checked for temporal completeness, spatial coverage, fallback hours, and consecutive gap length, and were not interpolated freely. Within the 2015–2017 historical archive used for model development, a small number of missing MRMS hours inside calibration or validation periods were reviewed against the surrounding observed basin-mean and basin-maximum rainfall; a documented, script-enforced repair rule set the target hour to exactly zero only when at least 8 surrounding evidence hours were available and all of them showed basin rainfall below a 0.001 mm dry threshold, with the repair, and its provenance, written to an audit record. This evidence-based gap repair was applied only to verified dry-hour gaps in the historical archive, never generically, and was never applied to the Florence event window itself. For the H-Q surrogate, USGS field measurements were paired with gauge observations only within a defined time-matching tolerance, and discharge-to-stage conversion was restricted to the range of discharge actually supported by the effective H-Q surrogate; values outside that observed range were not extrapolated.

3. Methodology

3.1 Software architecture and reproducibility

The workflow is implemented as a modular Python pipeline organized by processing stage: independent packages handle USGS observations and the H-Q surrogate (`observations/`), watershed and area-of-interest delineation (`spatial/`), terrain and DEM preparation (`terrain/`), precipitation acquisition and standardization (`rainfall/`), forcing assembly (`hydrology/`), the physically based and machine-learning discharge models together with shared subcatchment/routing utilities (`models/physics/`, `models/ml/`, `models/common/`), flood-inundation mapping (`flood_mapping/`), exposure and impact computation (`impact/`), a Florence-specific USGS/Physics/ML comparison utility, and an interactive dashboard front end. Each stage writes an explicit, versioned artifact (a parameter file, feature dataset, prediction series, or raster) that the next stage consumes, and quality-control scripts enforce structural checks – for example, that exactly 37 subcatchments are produced, that no development dataset contains rows on or after 1 January 2018, and that the production DEM resolution is within 5 cm of 1 m – before downstream steps are allowed to run. The full source tree is version-controlled and released alongside this manuscript (see Data and Code Availability) so that every quantitative claim in Sections 4 and 5 can be traced to a specific script and, where applicable, a specific retained parameter or metadata artifact.

3.2 Overview of the modelling workflow

The workflow proceeds in two linked stages. In the first stage, USGS observations are used to build a validated, event-effective H-Q surrogate; the upstream watershed and its 37 subcatchments are delineated; Florence and historical precipitation are processed and quality-controlled; and two independent discharge models are developed and applied to the Florence event. In the second stage, the resulting discharge time series are converted to stage, then to a spatially distributed water-surface elevation, compared with the lidar DEM under a hydraulic-connectivity constraint, and finally combined with population, land-cover, and infrastructure layers to quantify flood exposure. This sequencing – fixing the upstream drainage and routing structure before computing local flood extent and impacts – ensures that rainfall is converted to discharge in a hydrologically consistent manner before any local flood or exposure product is generated (Figure 2).

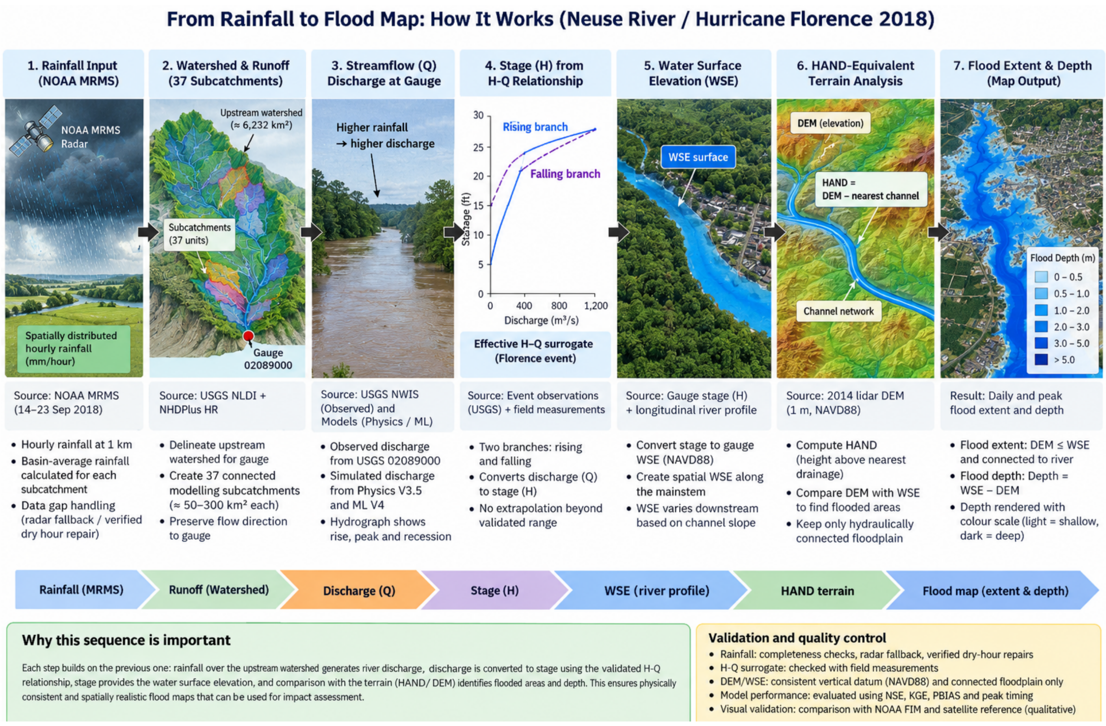

Figure 2: Conceptual end-to-end workflow from rainfall input through watershed routing, discharge prediction, stage conversion, water-surface-elevation mapping, height-above-nearest-drainage (HAND)-equivalent terrain interpretation, and final flood-extent and flood-depth output.

3.3 Effective stage-discharge (H-Q) surrogate

Because an authoritative historical rating table matching the exact hydraulic conditions of the Florence event was not available, an event-effective H-Q relationship was constructed directly from paired USGS observed discharge and gauge-height records at station 02089000 during the storm. Discharge and stage were paired by timestamp and separated into the rising and falling limbs of the hydrograph at the observed peak; repeated stage values within each limb were aggregated using the median discharge to suppress noise, and a monotonic isotonic regression was fitted independently to each limb's aggregated stage-discharge pairs, guaranteeing a physically consistent, non-decreasing stage-discharge relationship on each limb without imposing a parametric curve shape. Predictions were restricted to the interpolation range of each limb (no extrapolation), and both fitted limbs were checked against available USGS field measurements using root-mean-square error, mean absolute error, mean absolute percentage error, and the coefficient of determination as fidelity diagnostics before being used to convert modelled discharge into stage (Figure 3).

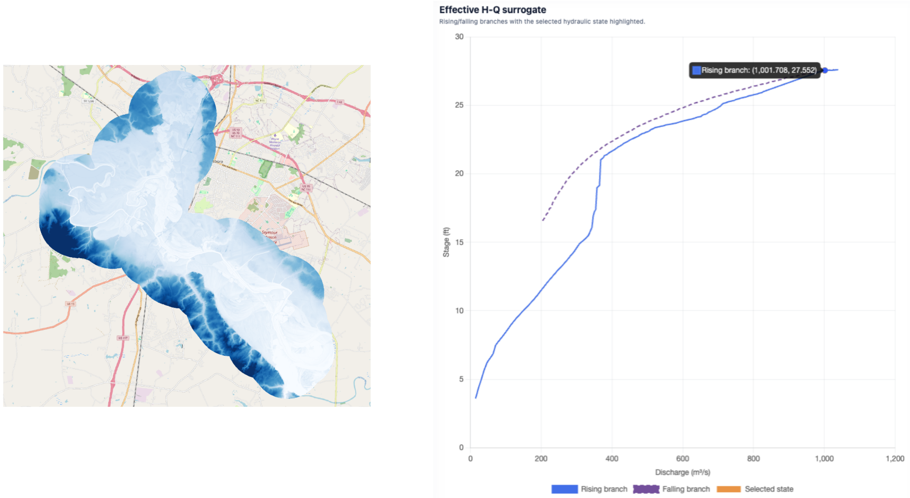

Figure 3: Left: production 1 m lidar digital elevation model for the Goldsboro area of interest (dark blue: low-elevation reach areas; light blue: higher-elevation reach areas). Right: effective, event-specific stage-discharge (H-Q) surrogate for USGS gauge 02089000 during Hurricane Florence, showing the separated rising branch (solid) and falling branch (dashed).

A terminological distinction is maintained throughout the workflow: an *H-Q branch* refers to the rising or falling side of the stage-discharge curve, reflecting flood hysteresis (the same discharge can correspond to a slightly different stage on the rising versus the falling limb because channel and floodplain storage differ), whereas a *workflow branch* refers to a separate processing path in the software pipeline, such as the parallel NOAA FIM reference-comparison branch. The flood mapper selects, for each day, the H-Q curve matching the hydrograph state (rising or falling) on that day; it does not average the two curves, and it does not extrapolate beyond the discharge range supported by the observed data (Figure 4).

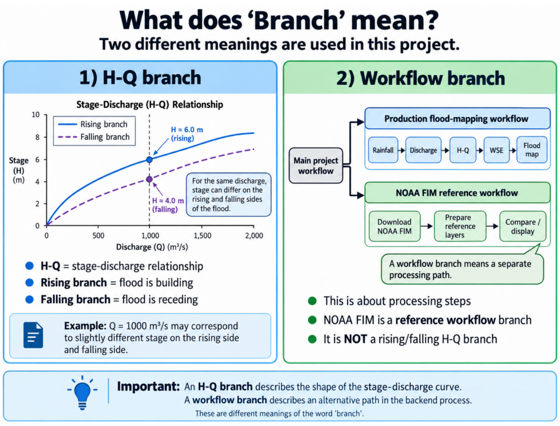

Figure 4: Illustration of the two distinct uses of the word "branch" in the workflow: (1) an H-Q branch describes the rising or falling side of the stage-discharge relationship; (2) a workflow branch describes an alternative processing path, such as the NOAA flood inundation mapping (FIM) reference comparison, within the software pipeline.

3.4 Watershed delineation and subcatchments

The upstream contributing watershed was delineated by querying the USGS NLDI for the land area draining to gauge 02089000, verifying that the returned gauge location and calculated drainage area were consistent with the USGS-published value of 2,399 mi^2. If a given NLDI request type was unavailable, an alternative NLDI option was used and accepted only after passing the same quality checks; the local Goldsboro mapping AOI was never substituted for the full upstream watershed. NHDPlus HR flowlines and raw catchments within the resulting watershed were aggregated into 37 connected modelling subcatchments using a target unit area of 150 km^2 with soft preferred bounds of 50–300 km^2; these bounds are a partitioning convenience for the routing discretization, not calibrated hydrologic parameters. Each subcatchment retains an explicit downstream routing path to the gauge, so that rainfall falling far upstream is delayed and routed through the network before contributing to discharge at Goldsboro (Figure 1).

3.5 Physics-based discharge model (Physics V3.5)

Physics V3.5 is a semi-distributed, conceptual rainfall-runoff model applied independently across the 37 subcatchments. It represents soil-moisture storage, evapotranspiration, saturation-dependent quick runoff, infiltration, slow drainage/baseflow, a moisture-dependent preferential interflow component, and downstream channel routing. Reference evapotranspiration is computed with the hourly FAO-56 Penman-Monteith equation (Allen et al., 1998),

$$\mathrm{ET}_0 = \frac{0.408\,\Delta\,(R_n - G) + \gamma\,\dfrac{37}{T+273}\,u_2\,(e_s - e_a)}{\Delta + \gamma\,(1 + 0.34\,u_2)}, \tag{1}$$

with wind speed adjusted to the standard 2 m reference height and the soil heat flux density G set to $0.10\,R_n$ during daylight hours and $0.50\,R_n$ at night, following standard FAO-56 practice. The distinguishing feature of version 3.5 relative to the retained V3.1 lineage is that the preferential (bypass) interflow fraction is made a function of relative soil wetness rather than held constant, becoming strongest when the soil is dry and progressively weaker as the soil wets, following:

$$\text{dryness} = \text{clip}\left(1 - \frac{S}{C},\, 0,\, 1\right) \tag{2}$$

$$f_{\text{pref,eff}} = f_{\text{pref,max}} \times \text{dryness} \tag{3}$$

$$\text{interflow}_{\text{input}} = \text{infiltration} \times f_{\text{pref,eff}} \tag{4}$$

where S is soil storage and C is soil capacity. No new parameter is introduced: the existing preferential-interflow fraction $f_{\text{pref,max}}$ is reinterpreted as a maximum, dry-state bypass fraction, bounded to $[0,\,0.15]$ (raised from the constant-fraction model's bound of 0.075, since the effective, moisture-scaled fraction is normally well below this ceiling). This change was adopted because a constant bypass fraction, calibrated against a dry-regime event, was found to overpredict discharge in a wetter validation event, indicating that a single fraction was too rigid across the range of antecedent wetness conditions represented in the historical event library. The V3.5 runtime is implemented and automatically verified as a structural, single-purpose source transformation of the retained V2/V3.1 simulation code, with a semantic preflight check confirming that exactly the intended equations changed before any calibration or prediction run is permitted.

Antecedent hydrological state was represented explicitly using a continuous June–September 2018 warm-up period together with ERA5-Land soil wetness and evapotranspiration data. The current, source-controlled production parameter set (Table 3; candidate 11 of a second, Florence-informed calibration round in which only soil capacity, the runoff-response exponent, and the quick-reservoir time constant were re-optimized relative to the preserved base V3.5 optimum) was used without further re-optimization for the Florence application, which keeps the Florence prediction fully reproducible. Model development used a retained event library of five historical calibration blocks (2015–2016) and three temporal-check blocks (2017), each spanning pre-event conditions, a 72-hour model warm-up, the rising limb and peak, and the recession (Table 4). Hurricane Florence itself was excluded from this calibration/validation library and was applied only afterward as the final, nominally independent event case.

Table 3: Physics V3.5 production parameter set (retained round-2 Candidate 11), as recorded in the version-controlled model artifact.

Parameter	Value
Soil capacity (mm)	592.5
Field capacity fraction (–)	0.85
Runoff-response exponent, β (–)	8.175
Soil drainage time constant (h)	1166.0
Quick-reservoir time constant (h)	76.22
Base (slow) reservoir time constant (h)	120.32
ET multiplier (–)	1.121
ET moisture exponent (–)	1.042
Channel velocity (m s^{-1})	0.201
Deep baseflow floor (mm h^{-1})	0.0694
Deep baseflow range (mm h^{-1})	0.0452
Preferential interflow fraction, dry-state maximum $f_{\mathrm{pref,max}}$ (–)	0.0762
Interflow reservoir time constant (h)	36.64

Table 4: Physics V3.5 retained event library: five 2015–2016 calibration blocks (C01–C05) and three 2017 temporal-check blocks (V01–V03). Hurricane Florence (2018) was excluded from this library.

Block	Role	Full date range (UTC)	Duration (h)
C01	Calibration	2015-11-16 17:00 → 2015-12-03 17:00	409
C02	Calibration	2015-12-29 22:00 → 2016-02-02 10:00	829
C03	Calibration	2016-02-03 07:00 → 2016-03-09 10:00	844
C04	Calibration	2016-05-05 20:00 → 2016-05-17 03:00	272
C05	Calibration	2016-10-05 08:00 → 2016-10-22 08:00	409
V01	Validation / temporal-check	2017-01-01 00:00 → 2017-01-16 06:00	367
V02	Validation / temporal-check	2017-05-20 20:00 → 2017-06-06 20:00	409
V03	Validation / temporal-check	2017-06-23 07:00 → 2017-07-10 07:00	409

The retained parameter artifact itself reports an approximate whole-event performance summary for Physics V3.5 against Hurricane Florence (Table 5); these values are documented in the released model metadata rather than independently recomputed for this manuscript, and the source metadata explicitly flags them as approximate.

Table 5: Approximate Florence-event performance metrics for Physics V3.5, as reported in the retained model artifact's metadata.

Metric	Reported value
Nash–Sutcliffe efficiency, NSE (–)	0.887
Kling–Gupta efficiency, KGE (–)	0.831
Percent bias, PBIAS (%)	+14.7
Peak-magnitude error (%)	−3.15
Peak-timing error (h)	+1.0

An important caveat applies to the interpretation of these Florence results, and is stated explicitly, in machine-readable form, in the released parameter artifact itself: the metadata record for Candidate 11 flags

```
florence_observed_q_used_for_selection = true
florence_independent_validation_after_this = false
```

That is, the current production parameter file was finalized during earlier project development, in which Florence observed discharge formed part of the historical information used during parameter selection. Consequently, the Physics V3.5 Florence metrics reported above and in Table 7 are best characterized as a model-application and comparison result rather than as a fully independent out-of-sample validation, in contrast to ML V4 (Section 3.6), for which Florence was strictly excluded from both training and candidate selection.

3.6 Machine learning discharge model (ML V4)

ML V4 is a gradient-boosted regression model (Chen & Guestrin, 2016) trained to predict hourly discharge at the Goldsboro gauge from a fixed set of 40 purely exogenous, causally available features, all derived from area-weighted basin rainfall and static routing geometry: (i) four basin-wide statistics per hour – the area-weighted mean, spatial standard deviation, spatial maximum, and area-weighted 90th percentile of subcatchment rainfall; (ii) four fractional-area terms giving the weighted fraction of basin area exceeding rainfall-intensity thresholds of 1, 2, 4, and 6 mm h^{-1}; (iii) five short-window rolling rainfall sums (3, 6, 12, 24, and 72 h) and five long-window rolling sums (7, 14, 30, 60, and 90 days, each requiring at least 99% of hours present in the window) of the basin-mean series; (iv) near/middle/far routing-zone rainfall, where subcatchments are assigned to a zone by a fixed 0.5 m s^{-1} diagnostic travel-time prior (near: $\leq$48 h; middle: 48–96 h; far: $>$96 h to the gauge), each zone contributing its own 1-hour mean plus 6-hour and 24-hour sums (nine features); (v) a routed-rainfall index computed at three advection velocities (0.25, 0.50, and 1.00 m s^{-1}) by lagging each subcatchment's rainfall by its travel time and re-averaging across subcatchments subject to a minimum 99% routed-area-coverage requirement, again with 1-hour, 6-hour, and 24-hour sums at each velocity (nine features); and (vi) four seasonal terms, the sine and cosine of day-of-year and of hour-of-day. By design, the feature set excludes any observed-discharge lag, future rainfall, or recursively fed predicted-discharge state, so that every hourly prediction is generated directly (non-recursively) from information that would have been available at prediction time.

The model was trained on hourly data from 10 May 2015 through 1 January 2017 and evaluated for model selection using the same three 2017 temporal-check events used for the physics model (through 1 January 2018), with Hurricane Florence excluded from both training and candidate selection. Ten predefined XGBoost hyperparameter configurations were compared (Table 6), each combining a maximum tree depth, learning rate, ensemble size, minimum child weight, subsample and column-subsample fractions, L1/L2 regularization strengths, a target transform (raw, square-root, or log1p), and a high-flow sample-weighting scheme, using a squared-error training objective, root-mean-square-error evaluation metric, and a histogram-based tree-growing method. High-flow observations were up-weighted during training using one of three predefined quantile-based schemes, which assign successively larger weights (up to 6–10$\times$ the base weight) to hours above the empirical 75th, 90th, and 95th percentiles of training discharge, so that flood peaks were not dominated by the much larger number of low-flow hours.

Each candidate was scored using validation Nash–Sutcliffe efficiency (NSE) (Nash & Sutcliffe, 1970), Kling–Gupta efficiency (KGE) (Gupta et al., 2009), percent bias (PBIAS), peak-magnitude error, and peak-timing error via the composite metric

$$s = 0.30\,\mathrm{NSE} + 0.25\,\mathrm{KGE} - 0.15\,\frac{|\mathrm{PBIAS}|}{100} - 0.20\,\frac{|\text{peak error}|}{100} - 0.10\,\min\left(\frac{|\text{peak timing error (h)}|}{72},\,2\right), \tag{5}$$

computed once on the pooled 2017 validation record (s_{pooled}) and once per individual validation event ($s_{\text{event},i}$), and combined into a robustness-weighted selection score

$$S = 0.35\,s_{\text{pooled}} + 0.45\,\overline{s_{\text{event}}} + 0.20\,\min_{i}\,s_{\text{event},i}, \tag{6}$$

so that a candidate could not be selected on the strength of strong pooled performance alone if it performed poorly on any single validation event. The selected candidate was additionally required to satisfy minimum quality gates on the pooled validation record (NSE ≥ 0.30, KGE ≥ 0.30, $|\mathrm{PBIAS}| \leq 30\%$, $|$peak error$| \leq 40\%$) before being accepted for the Florence application.

Table 6: ML V4 candidate hyperparameter grid. Weight schemes W1/W2/W3 apply multipliers of (1.0, 1.5, 3.0, 6.0), (1.0, 2.0, 4.0, 8.0), and (1.0, 2.5, 5.0, 10.0) to observations below the 75th, between the 75th–90th, 90th–95th, and above the 95th percentile of training discharge, respectively.

ID	Depth	LR	Trees	Min. child	Subsample	Colsample	L_2	Transform	Weights
V401	2	0.030	700	20	0.85	0.85	10.0	sqrt	W1
V402	3	0.025	800	15	0.85	0.85	8.0	sqrt	W1
V403	3	0.030	700	10	0.90	0.85	5.0	sqrt	W2
V404	4	0.020	900	10	0.90	0.80	5.0	sqrt	W2
V405	2	0.030	700	15	0.85	0.85	8.0	raw	W1
V406	3	0.025	800	10	0.90	0.85	5.0	raw	W2
V407	4	0.020	900	8	0.90	0.80	3.0	raw	W3
V408	2	0.035	700	15	0.85	0.85	8.0	log1p	W1
V409	3	0.030	750	10	0.90	0.85	5.0	log1p	W2
V410	4	0.020	900	8	0.90	0.80	3.0	log1p	W3

3.7 Flood inundation mapping

For each day in the 14–23 September 2018 window, the maximum daily discharge from a chosen source (USGS observed, Physics V3.5, or ML V4) was classified as occurring on the rising or falling side of that source's hydrograph, and converted to stage using the matching H-Q curve (Section 3.3). Stage was converted to an absolute gauge water-surface elevation (WSE) by adding the 41.926 ft NAVD88 gauge datum:

$$\mathrm{WSE}_{\text{gauge}}\ (\text{ft NAVD88}) = 41.926 + H\ (\text{ft}) \tag{7}$$

A longitudinal WSE profile was then constructed along the named Neuse River mainstem by sampling DEM elevation at regular intervals along the channel centerline and fitting a single along-channel slope by iteratively re-weighted linear regression: at each iteration the residuals between sampled elevation and the fitted line are used to compute a median-absolute-deviation (MAD)-based robust scale ($1.4826 \times \mathrm{MAD}$), samples beyond this robust window are down-weighted or excluded, and the fit is repeated until convergence or a minimum-retained-sample floor is reached. The fitted slope is applied only along the channel (longitudinal) direction, with no lateral (cross-valley) tilt of the water surface, and is rejected by an automatic safety check if it exceeds a maximum plausible longitudinal slope, guarding against DEM/vector misalignment. This profile allows the water surface to vary both upstream and downstream of the gauge within the Goldsboro AOI rather than treating the gauge elevation as a single flat plane across the domain.

Every valid cell of the 1 m lidar DEM was compared against this spatial WSE; a cell was classified as a flood candidate only where ground elevation was at or below the local water surface. Hydraulic connectivity was then enforced using morphological binary propagation (a mask-constrained, 8-connected geodesic reconstruction) seeded from a narrow buffer around the mainstem centerline: only candidate cells reachable from this seed through other candidate cells were retained in the final flood extent, so that isolated, unconnected low-lying depressions were excluded even though they satisfied the elevation criterion alone. Flood depth for each retained cell was computed as

$$\text{Depth}(x) = \max\big(0,\ \text{WSE}(x) - \text{DEM}(x)\big). \tag{8}$$

The developers of this component explicitly characterize it as a terrain-based, connectivity-constrained "bathtub" approximation to inundation extent – efficient and reproducible at 1 m resolution over a multi-day event window – rather than a solution of the shallow-water (or any other) hydrodynamic equations; it does not represent momentum, backwater, or time-varying wave propagation within the floodplain. A height-above-nearest-drainage (HAND)-style terrain metric (Rennó et al., 2008; Nobre et al., 2011) was also computed and displayed as an interpretive aid on the project dashboard; however, the production flood-extent and flood-depth calculation itself is based on the direct comparison of absolute spatial WSE against the lidar DEM together with mainstem hydraulic connectivity, not on a single HAND threshold applied uniformly across the AOI.

3.8 Impact and exposure assessment

Flood-exposure estimates were derived by overlaying the daily flood-depth rasters with WorldPop 2018 gridded population, NLCD 2016 land cover and imperviousness, and OpenStreetMap (OSM) building, road, and facility layers. Population and land-cover exposure were computed as the fraction of each native WorldPop and NLCD grid cell covered by the flood polygon – reprojected and resampled as a continuous coverage fraction on each dataset's own grid rather than collapsed to a binary in/out mask – so that cells straddling the flood boundary contribute partial, area-weighted exposure instead of being wholly included or excluded. Road exposure was computed by an exact geometric intersection of each OSM road line with the flood polygon, yielding the true clipped sub-segment length within the flood extent (rather than selecting whole road segments that merely touch the polygon), which was then aggregated per road and per facility. Because WorldPop (2018) and NLCD (2016) are event-era proxy datasets rather than event-synchronous observations, and because the OSM extract reflects current infrastructure rather than a historical snapshot unless separately replaced, the resulting impact outputs are interpreted as flood-exposure estimates conditioned on those specific source vintages, not as a certified post-event damage assessment.

4. Results

4.1 Discharge prediction performance

Table 7 compares daily USGS-observed discharge at gauge 02089000 with the Physics V3.5 and ML V4 predictions over the 14–23 September 2018 window. Both models reproduced the overall rise, peak, and recession shape of the observed hydrograph and correctly identified 18 September 2018 as the date of peak discharge, consistent with the observed record. Physics V3.5 achieved a lower daily discharge mean absolute error (82.3 $m^3\ s^{-1}$) than ML V4 (103.6 $m^3\ s^{-1}$) and a lower daily stage mean absolute error (1.03 ft versus 2.01 ft) over the same window. On the observed peak date, Physics V3.5 predicted a discharge of 1001.0 $m^3\ s^{-1}$ and a stage of 27.55 ft, compared with an ML V4 prediction of 897.8 $m^3\ s^{-1}$ and 27.04 ft, against an observed discharge of 1039.2 $m^3\ s^{-1}$ and stage of 27.60 ft.

Table 7: Daily USGS-observed discharge compared with Physics V3.5 and ML V4 predictions at gauge 02089000, 14–23 September 2018.

Date	**USGS observed Q ($m^3\ s^{-1}$)**	**Physics V3.5 Q ($m^3\ s^{-1}$)**	**ML V4 Q ($m^3\ s^{-1}$)**
2018-09-14	268.44	108.01	89.05
2018-09-15	376.61	383.05	169.54
2018-09-16	478.55	674.17	455.79
2018-09-17	826.85	936.69	823.65
2018-09-18	1039.23	1001.03	897.80
2018-09-19	1036.40	1000.12	891.27
2018-09-20	942.95	942.67	760.78
2018-09-21	792.87	841.70	743.65
2018-09-22	637.13	734.97	607.94
2018-09-23	509.70	638.50	586.17
Summary statistics, 14–23 September 2018			
Daily discharge MAE ($m^3\ s^{-1}$)	–	**82.26**	103.60
Daily stage MAE (ft)	–	**1.030**	2.011
Observed-peak date	2018-09-18	2018-09-18	2018-09-18
Q on observed-peak date ($m^3\ s^{-1}$)	1039.23	1001.03	897.80
Stage on observed-peak date (ft)	27.600	27.552	27.040

Figure 5 shows the daily evolution of observed discharge together with the branch-derived stage, gauge water-surface elevation, and HAND-equivalent threshold over the event window, and Figure 6 shows the corresponding 24-hour MRMS rainfall accumulation. Consistent with the expected rainfall-runoff response, basin-mean and basin-maximum rainfall peaked on 14–15 September and again, at a lower secondary maximum, on 17 September, whereas discharge and water-surface elevation continued to rise through 18–19 September and remained elevated through 20–23 September even after daily rainfall had returned to near zero, reflecting the delayed basin response associated with infiltration, storage, and channel routing across the 37-subcatchment network.

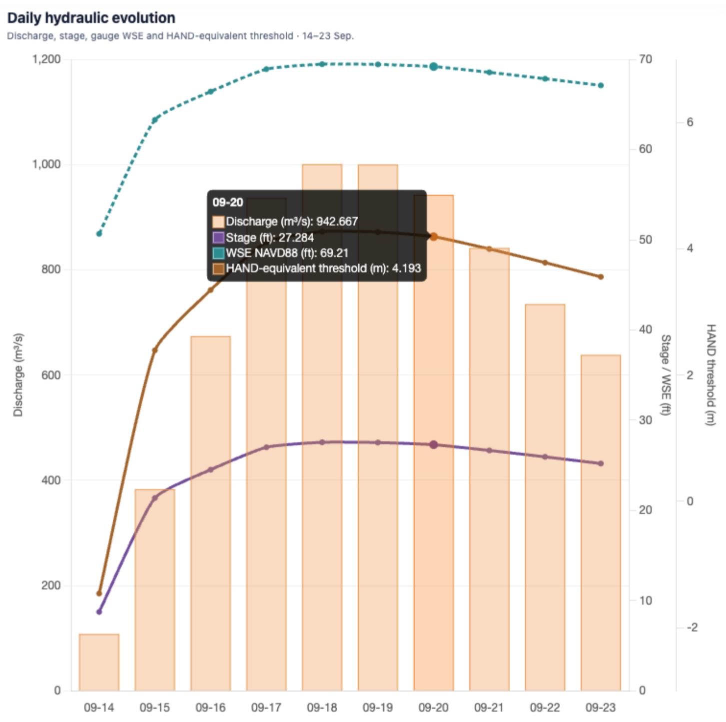

Figure 5: Daily observed discharge, branch-derived stage, gauge water-surface elevation (WSE, NAVD88), and HAND-equivalent threshold at USGS gauge 02089000, 14–23 September 2018.

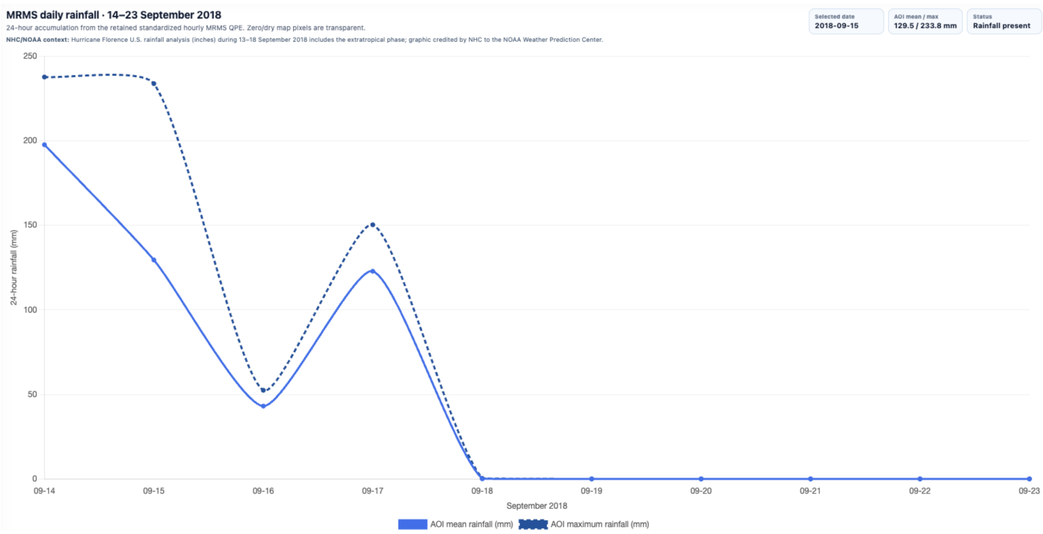

Figure 6: Daily (24-hour) area-of-interest mean and maximum Multi-Radar Multi-Sensor (MRMS) rainfall accumulation, 14–23 September 2018.

4.2 Flood inundation extent and depth

Daily flood-extent and flood-depth rasters were generated for the Goldsboro AOI by comparing the spatial water-surface-elevation profile with the 1 m lidar DEM under the mainstem hydraulic-connectivity constraint described in Section 3.7. Figure 7 shows the resulting flood-depth product together with the corresponding upstream-watershed and Goldsboro-AOI boundaries, illustrating that the connected inundation footprint follows the Neuse River mainstem and its immediately adjacent low-lying floodplain both upstream and downstream of the gauge, consistent with the longitudinal WSE profile approach.

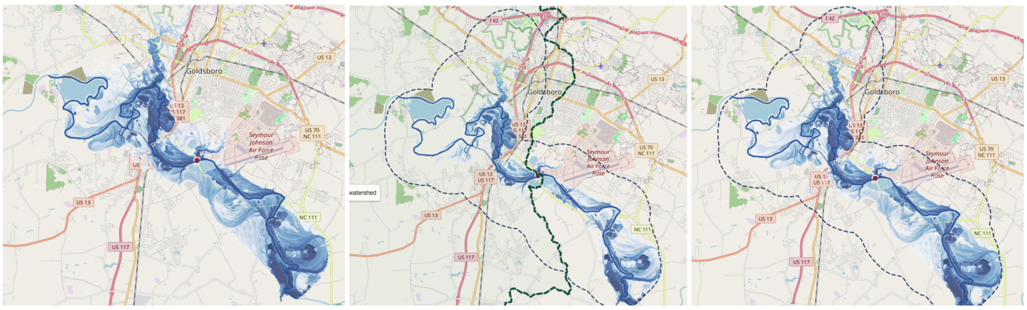

Figure 7: Flood-depth map over the Goldsboro area of interest. Darker blue indicates greater calculated water depth; transparent areas are dry or fall outside the valid flood-depth display. Panels show the mapped extent together with the upstream-watershed (dashed) and local area-of-interest boundaries.

4.3 Exposure and impact assessment

Overlaying the mapped flood extent with OSM road data indicates substantial exposure of the local road network within the Goldsboro AOI, including segments near Seymour Johnson Air Force Base and along US 13, US 70, US 117, and NC 111 (Figure 8, left panel). The corresponding land-cover overlay shows that a large proportion of the inundated area corresponds to developed land and cultivated or managed land cover along the Neuse River floodplain (Figure 8, right panel). As noted in Section 3.8, these exposure estimates should be interpreted in light of the specific vintages of the underlying population, land-cover, and infrastructure datasets rather than as an exact, event-synchronous damage assessment.

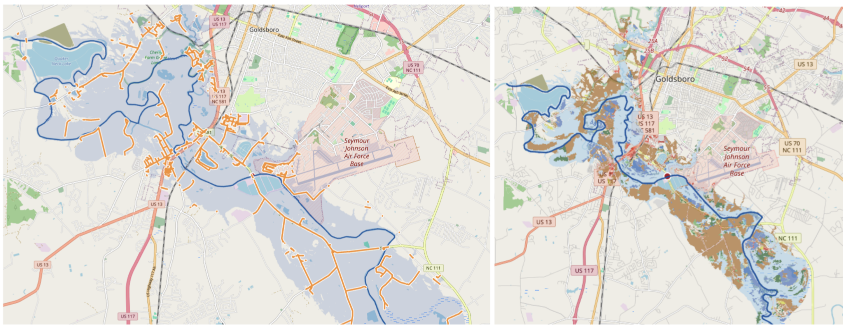

Figure 8: Left: roads (orange) intersecting the mapped flood extent within the Goldsboro area of interest. Right: land-cover classes intersecting the mapped flood extent.

5. Discussion

The results indicate that, for the Hurricane Florence event at Goldsboro, the semi-distributed physics-based model (Physics V3.5) reproduced observed discharge and stage more closely than the purely exogenous, feature-based machine learning model (ML V4), by roughly 21 m^3 s^{-1} in daily discharge mean absolute error and about one foot in daily stage mean absolute error. Both models nonetheless captured the overall shape and peak timing of the flood hydrograph, and ML V4's more conservative (lower) discharge estimates on the rising limb and near the peak are consistent with the known tendency of tree-based, non-extrapolating regression methods to under-predict values that lie near or beyond the upper range of their training distribution, since Hurricane Florence was deliberately withheld from ML

V4's training and candidate-selection data.

This comparison should, however, be interpreted with an important asymmetry in mind: the Physics V3.5 production parameter set was finalized during earlier development using historical information that included Florence's own observed discharge, so its Florence result is best described as a model-application and comparison outcome rather than a fully independent validation, whereas ML V4's Florence prediction reflects a genuinely held-out evaluation. This asymmetry is not a post-hoc inference on the author's part: it is recorded directly, in machine-readable form, in the released parameter artifact's own metadata (see the quoted metadata flags in Section 3.5), and it means the discharge comparison in Table 7 – and the approximate NSE/KGE figures in Table 5 – should not be read as unambiguous evidence that physically based models generalize better than machine learning models to unseen extreme events in this basin. A fairer comparison would require a physics model whose parameters were also strictly withheld from any information about the Florence event; the ML V4 protocol used here (Section 3.6) demonstrates that such a strictly held-out design is achievable within the same pipeline, and could in principle be applied retrospectively to a re-calibrated physics model in future work.

The flood-mapping approach adopted here – comparing an absolute, longitudinally varying water-surface elevation against a high-resolution lidar DEM under a morphologically enforced mainstem-connectivity constraint – avoids two common sources of error in simplified flood mapping: the use of a single flat-plane water elevation across a spatially extensive AOI, and the inclusion of hydraulically disconnected, low-lying depressions as false-positive flood cells. As the implementation itself makes explicit, this remains a terrain-based, connectivity-constrained "bathtub" approximation rather than a hydrodynamic solution, so it cannot represent momentum effects, backwater from downstream constrictions, or the time lag of a flood wave propagating through the floodplain itself (as opposed to through the channel network feeding it); it is best suited to slow-rising, quasi-steady events such as Florence rather than flash floods with strong short-term dynamics. The HAND-equivalent terrain metric computed for the project dashboard is a useful qualitative aid for interpreting relative floodplain terrain, but it was deliberately not used as the sole or uniform threshold for the production flood-extent calculation, which instead relies on the mainstem-connected WSE-DEM comparison. Similarly, computing exposure as a fractional, sub-pixel overlap on each dataset's native grid, and clipping roads by exact geometric intersection rather than whole-segment selection, reduces a common source of over- or under-counting in simplified exposure overlays, though it does not address the dataset-vintage limitation discussed next.

Several limitations should be considered when using or extending these results. First, in the absence of an authoritative historical rating table exactly matching the Florence event, the H-Q surrogate used here is itself an approximation built from event observations and field measurements, and its validity is bounded by the observed discharge range; the workflow deliberately avoids extrapolating stage estimates beyond that range. Second, the historical MRMS archive used for model development contains data gaps that were filled only under strict, evidence-based dry-hour criteria, and any residual, unflagged gaps could subtly influence the historical calibration and validation statistics. Third, the exposure assessment combines datasets of different vintages (WorldPop 2018, NLCD 2016, and a current OSM snapshot), so the reported exposure figures characterize flood-exposure potential under those source vintages rather than a certified, event-synchronous damage assessment. Finally, both discharge models and the flood-mapping product are specific to a single gauge and a single, if extreme, historical event; transferability to other basins or to design storms outside the historical envelope used here would require additional validation.

6. Conclusion

This study developed and applied a coupled physics-based/machine-learning discharge modelling and flood-mapping workflow for the Neuse River at Goldsboro, North Carolina, during Hurricane Florence (September 2018). An event-effective, hysteresis-aware stage-discharge surrogate was constructed directly from observed hydrometric data, and two independently developed discharge models – a semi-distributed physical model and an XGBoost-based machine learning model – were compared under an explicit temporal calibration/validation design. Over the ten-day evaluation window, the physics-based model produced a lower discharge and stage error than the machine learning model, while both models correctly identified the timing of the observed peak. The resulting discharge series were converted into a spatially explicit, mainstem-connected flood-depth product using a 1 m lidar DEM, and combined with population, land-cover, and infrastructure datasets to characterize flood exposure in the Goldsboro area of interest. The workflow illustrates a transparent, reproducible approach to extreme-event flood mapping in a data-scarce, single-gauge setting, and highlights the importance of clearly documenting data-gap handling, model validation independence, and dataset vintage assumptions when such workflows are used to support flood-risk communication or emergency-response decision-making.

Data and Code Availability

The data-processing and modelling scripts developed for this study are available at `https://github.com/asadpstu/hurricane-florence`. Underlying observational data are publicly available from the USGS National Water Information System, USGS NHDPlus HR, NOAA/NCEP MRMS, the Copernicus Climate Data Store (ERA5-Land), WorldPop, the National Land Cover Database, and OpenStreetMap, as referenced in Table 2.

Author Contributions

H. M. Ashaduzzaman conceived the study, developed the modelling and flood-mapping workflow, performed the analysis, and wrote the manuscript.

Conflicts of Interest

The author declares no conflict of interest.

References

Allen, R. G., Pereira, L. S., Raes, D., & Smith, M. (1998). *Crop Evapotranspiration: Guidelines for Computing Crop Water Requirements*. FAO Irrigation and Drainage Paper 56. Food and Agriculture Organization of the United Nations, Rome.

Chen, T., & Guestrin, C. (2016). XGBoost: A scalable tree boosting system. In *Proceedings of the 22nd ACM SIGKDD International Conference on Knowledge Discovery and Data Mining* (pp. 785–794). Association for Computing Machinery.

Gupta, H. V., Kling, H., Yilmaz, K. K., & Martinez, G. F. (2009). Decomposition of the mean squared error and NSE performance criteria: Implications for improving hydrological modelling. *Journal of Hydrology*, 377(1–2), 80–91.

Nash, J. E., & Sutcliffe, J. V. (1970). River flow forecasting through conceptual models, part I – A discussion of principles. *Journal of Hydrology*, 10(3), 282–290.

Nobre, A. D., Cuartas, L. A., Hodnett, M., Rennó, C. D., Rodrigues, G., Silveira, A., Waterloo, M., & Saleska, S. (2011). Height Above the Nearest Drainage – a hydrologically relevant new terrain model. *Journal of Hydrology*, 404(1–2), 13–29.

Rennó, C. D., Nobre, A. D., Cuartas, L. A., Soares, J. V., Hodnett, M. G., Tomasella, J., & Waterloo, M. J. (2008). HAND, a new terrain descriptor using SRTM-DEM: Mapping terra-firme rainforest environments in Amazonia. *Remote Sensing of Environment*, 112(9), 3469–3481.